28

Three-Dimensional Patterning using Ultraviolet Nanoimprint Lithography

Maan M. Alkaisi and Khairudin Mohamed
MacDiarmid Institute for Advanced Materials and Nanotechnology,
Department of Electrical and Computer Engineering,
University of Canterbury, Christchurch 8014,
New Zealand

1. Introduction

Although an extensive number of publications have been reported on nanoimprint lithography (NIL) techniques, the ability of NIL for three-dimensional (3-D) patterning has not been fully addressed in terms of the mold fabrication and imprint processes. Developing technologies for patterning 3-D and multilevel features are important because they eliminate multiple steps and complex interlevel alignments in the fabrication process of nanoscale devices and structures.

The semiconductor industries through the International Technology Roadmap for Semiconductor (ITRS) organization have identified NIL (ITRS 2003; ITRS 2008), especially ultraviolet curable nanoimprint lithography (UV-NIL) as a strong candidate for the next generation lithography (NGL) technology for nodes down to 5 nm.

Three dimensional NIL (3D-NIL) will have a variety of practical applications including generating patterns for MEMS and NEMS devices, on-chip optics, antireflection structures and in biochip reactors.

This chapter explores the 3-D patterning capability using an UV-NIL technique. The 3-D features and multilevel mold design, fabrication, and imprint processes have been studied and analysed and outcome will be presented and discussed.

In the UV-NIL technique, a transparent mold with micro/nanostructure patterns on its surface is allowed to be printed and replicated on UV curable polymer without the need of high applied pressure or temperature. UV-NIL has the potential to fabricate micro/nanostructures with high resolution, high reproducibility, low cost, high throughput and in addition is capable of 3-D patterning. Its resolution is not limited by diffraction as in optical lithography or electron scattering as in electron beam lithography (EBL) and there is no expense that scales with reducing dimensions as in other nanolithography technologies.

The UV-NIL technique is especially useful in avoiding processes that require high pressure and high temperature cycles. Mold pattern writing, pattern transfer and imprint are the three major areas that are described here. The master molds or dies are made using a high-resolution but low-throughput EBL technique. The pattern transfer process for making the mold is achieved using a reactive ion etching (RIE) technique and subsequent imprint lithography is employed for the replication of the micro/nanostructures onto the daughter molds.

Source: Lithography, Book edited by: Michael Wang,
ISBN 978-953-307-064-3, pp. 656, February 2010, INTECH, Croatia, downloaded from SCIYO.COM

The 3-D pattern profiles are created on a negative photoresist using a Raith 150 EBL tool in a single step variable e-beam dose controlled exposure. Resist contrast curves are obtained with a negative photoresist (ma-N2403) and a single pass line (SPL) pattern writing scheme is employed to create the 3-D pattern profiles. Specially designed test patterns are used to demonstrate the capability of UV-NIL in replicating the 3-D and multilevel structures.
Surface charging, electron back scattering and proximity effects during e-beam exposure are the main factors influencing pattern writing on insulating materials such as quartz. Multiple approaches for suppressing the charging, electrons backscattering and proximity effects will be presented in section 3.2. Monte Carlo simulation using CASINO software is employed to investigate the effects of accelerating voltages on electron trajectories during the e-beam exposure.
As a substrate material that has numerous applications at micro/nano scale, quartz is the most common choice for many optical device applications. It is widely used as a UV transparent imprint mold. 3-D pattern transfer onto quartz substrate will be described in section 3.3. The optimization process to achieve a very low surface roughness of below 5 nm suitable for UV exposure and faithful pattern transfer will be presented in section 3.4. In this section an indepth explanation of the underlying science of etching hard and insulating materials such as quartz will be discussed.

2. Research background

In general, 3-D micro/nanostructures, including 3-D NIL molds, can be fabricated using various techniques such as multistep lithography , maskless gray-scale lithography (Totsu et al. 2006), FIB writing (Taniguchi et al. 2006), proton beam writing (Simcic et al. 2005) , x-ray lithography (Romanato et al. 2003); (Romanato et al. 2004) , or combination of EBL and dry etching. These techniques are high cost, low throughputs and some suitable only for relatively large features and not for nanoscale applications. Another method of fabricating 3-D structures is by the surface texturing technique using either dry plasma RIE process (Kumaravelu et al. 2004) or wet chemical etching. A 3-D sub-wavelength surface texturing can also be fabricated using interferometric lithography patterning followed by RIE (Chiu et al. 2006) but these are used for periodic patterns only. As indicated 3-D patterns with structures down to sub-wavelength scale can be fabricated using a number of advanced lithography techniques, however, their reproducibility in mass production, low cost environment is the major limitation.
In EBL, patterns are normally created in a graphic or layout design software such as L-Edit. The patterns may be grouped in multiple clusters called design layer based on their feature sizes, electron dose and acceleration voltage. For 3-D patterning, there are two approaches for defining the patterns: variable acceleration voltage and variable exposure dosage. The variable acceleration voltage technique (Ishii & Taniguchi 2007) uses a specific voltage assigned to a specific pattern design layer where the limitation is set on the maximum number of the possible assigned design layers. When a positive resist such as PMMA is exposed to the e-beam, the depth of the e-beam penetration is determined by the e-beam accelerating voltage as illustrated in Figure 1(a). In this method, for example, the depths of the developed 3-D pattern are controlled by the magnitude of the uniform accelerating voltage assigned to each pattern layer. After pattern development, the depths of the trenches formed are a factor of the uniform accelerating voltage assigned to each design layer.

On the other hand, the variable dosage technique employs an e-beam exposure approach with path by path routing using a single pass line (SPL) scheme, with a specifically assigned dosage for each path as illustrated in Figure 1(b). In this method everything are designed in a single design layer. The 3-D profiles can be achieved on negative resist by bringing the SPL paths close (but not less than e-beam spot size) and parallel to each other. There is no limitations on the number of paths and all paths are designed in a single design layer for any 3-D pattern design (Mohamed et al. 2007).

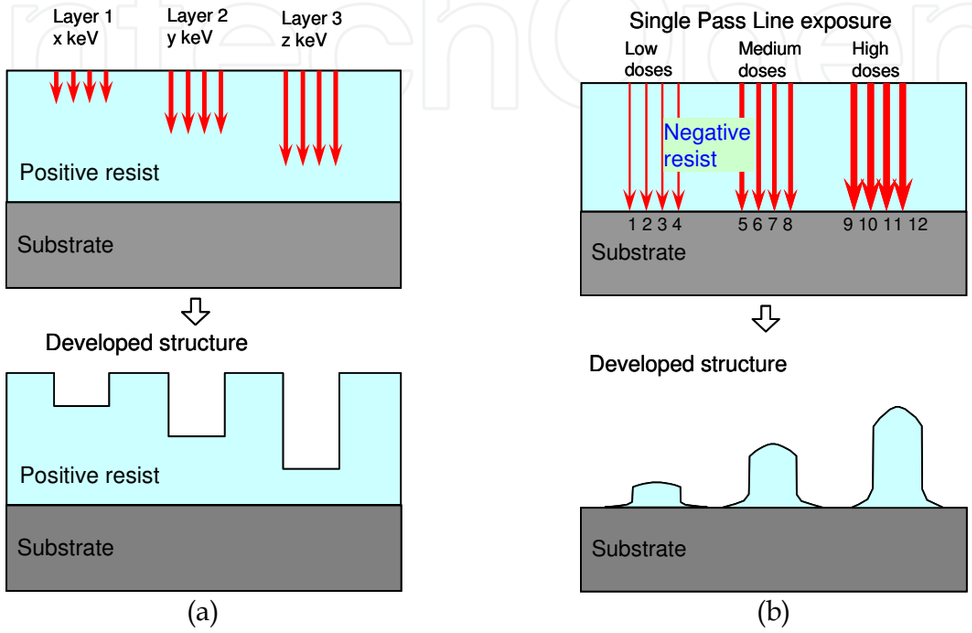

Fig. 1. The two different methods of 3-D patterning using the EBL technique, (a) variable accelerating voltages and (b) variable e-beam dosages.

For 3-D patterning, negative resist such as ma-N2403 from Microresist Technology GmbH can be used for this purpose. Previous work (Konijn et al. 2005) has shown some encouraging results for 3-D and multilevel structures on other resist system. An experiment was designed to study the relationship between the e-beam dosages and the effects of electrons backscattering and proximity effects onto the developed ma-N2403 resist profile. A single pass line (SPL), double pass lines (DPL) and quadruple pass lines (QPL) schemes with various e-beam dosages range were attempted. For parallel multiple line exposure, the spacing between the lines' exposures were about 20 nm to 30 nm. In a group of uniform dosages for each exposure lines, it was observed that the middle of the developed resist structures received higher exposure dosages because of the electrons' backscattering and proximity effects. Figure 2(a) shows an AFM trace of resist cross sections for a range of uniform dosages applied to a QPL exposure scheme. It shows that the remaining resist thickness after development is a factor of the dosages applied.

Figure 2(b) illustrates the contrast curve of the negative resist ma-N2403 when exposed with SPL, DPL and QPL exposure schemes. The SPL, DPL and QPL curves represent an exposure conditions with zero, medium and high proximity effects respectively. There were large differences in the structure height between SPL and DPL writing schemes. For no proximity effect as in SPL, the structure heights were very low. These data have been used for estimating the required dosage factors in designing a 3-D pattern.

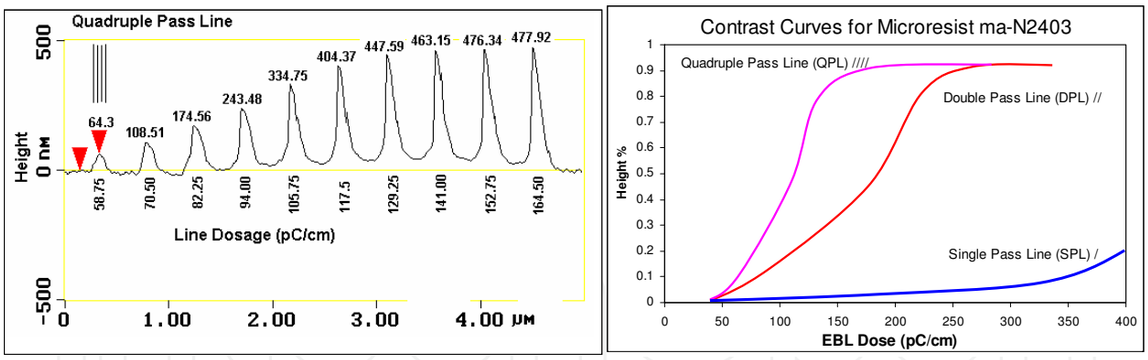

(a) (b)

Fig. 2. (a) AFM traces of the developed ma-N2403 after being exposed with a range of e-beam dosages using QPL scheme and (b) the contrast curves of negative resist ma-N2403 for SPL, DPL and QPL exposure schemes.

3. Mold fabrication

The three-dimensional mold fabrication involves writing a 3-D profile on negative photoresist and then directly transfers the pattern using single-step RIE process. The creation of the 3-D geometrical shapes such as pyramid, hemisphere, cone and other complex shapes will be described in this section. These 3-D structures have many applications especially in optical devices.

A subtractive pattern transfer method (RIE) was employed because the 3-D patterns have to be directly transferred onto the mold substrate in a single-step RIE process to simplify the mold making process. A negative photoresist is employed as a 3-D imaging and masking layer for the EBL and RIE process repectively.

New fabrication processes have been developed by the present work in order to suppress the surface charging effects during the EBL 3-D pattern writing on insulating substrates. Since the 3-D mold fabrication requires direct pattern transfer from mask to substrate, depositing a thin metal coating on the substrate-resist interface as a charge dissipation/grounding layer was not possible. Depositing a thin metal layer on top of the negative resist surface as a charge dissipation/grounding layer was also ruled out. Acidic solution used to remove the thin metal layer prior to pattern development process caused polymer crosslinking on the negative resist surface (Thackeray et al. 1989); Shaw et al., 1997). As a result, no subsequent development process would be possible. For these reasons, the use of conductive polymers was investigated as will be illustrated in the following section 3.2.2.

3.1 Mold design and preparation

The 3-D pattern layout was designed using Raith-150 EBL pattern layout software where the single pass line (SPL) writing scheme is utilised. Figure 3(a) shows an example of a writing scheme for a hemispherical shape. Every SPL path/route was assigned with an individual dosage which was defined through the optimisation process. The spacing between lines is about 20 nm to 30 nm. The developed resist profile is the combined result of proximity effects, back scattering and e-beam dosages. To achieve the desired profile, a trial and error method was employed to optimise the e-beam dosages after a number of experimental

cycles to satisfy the profiles. Figure 3(b) shows another example of a writing scheme for a pyramid profile with a similar method.

The negative tone photoresist from Microresist Technology, ma-N2403 was spun coated on a cleaned quartz substrate at 3000 rpm for 30 seconds and pre-baked in an oven at a temperature of 95 ^{o}C for 30 minutes to achieve a 600 nm layer thickness.

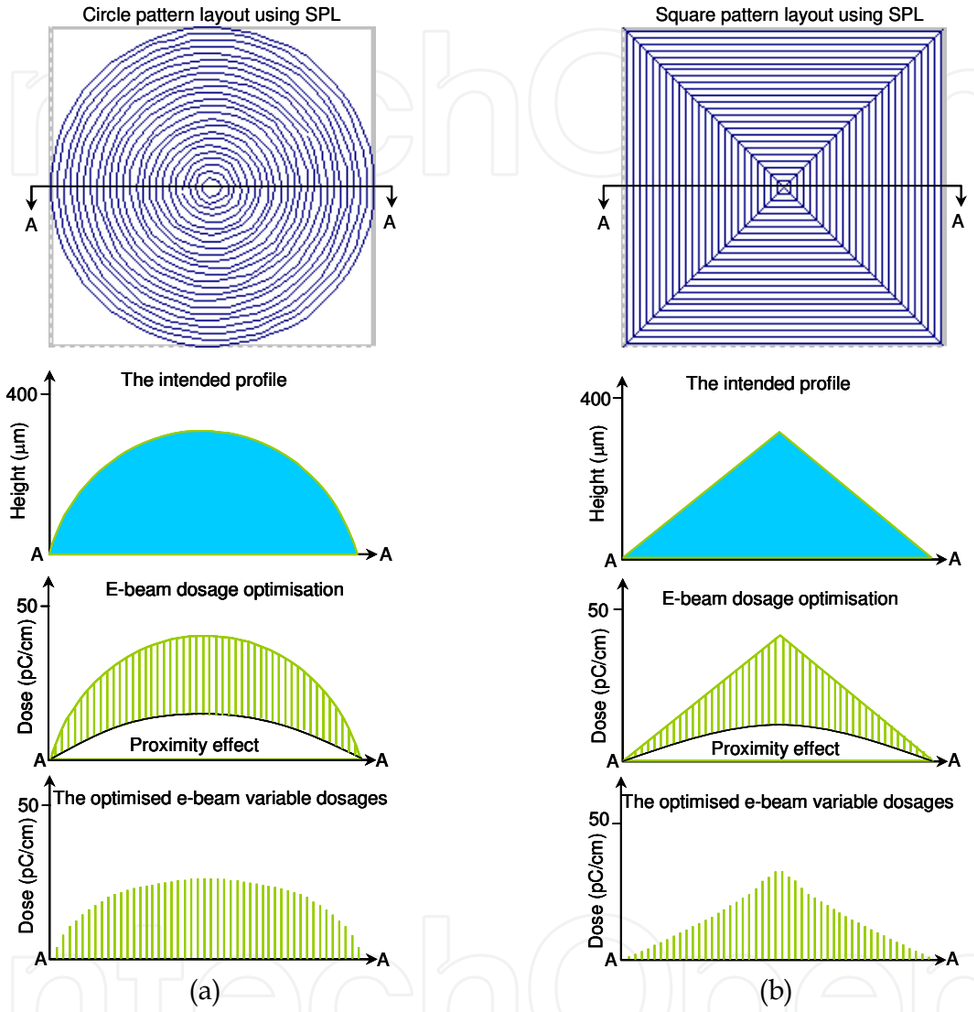

Fig. 3. The SPL writing scheme for 3-D patterns. (a)hemisphere and (b) square base pyramid.

3.2 Fabrication techniques

As mentioned earlier, surface charging is one of the major challenges in patterning on insulating substrate such as quartz. This is even more complicated when the required pattern is in 3-D. Surface charging trapped near the insulating surfaces causes great difficulties in focusing the e-beam onto the resist surface and the unbalanced surface potential of the resist deflects the beam and causes severe pattern distortion (Joo et al. 2006).

Two fabrication approaches were developed to minimise this problem. The first approach is applying e-beam at low accelerating voltages (low keV). The use of low keV leads to reduced beam interaction volume. The penetration depth of the electrons into insulating

materials/substrates is much less than higher keV electrons. Based on this approach a 3-D fabrication method called called Critical Energy (CE) or Critical Accelerating Voltage method was developed and followed (Mohamed et al. 2007). In the CE method as illustrated in Figure 4(a), a variable controlled e-beam dosages at an optimised low accelerating voltage is employed in 3-D pattern writing on a negative resist using EBL. The developed pattern is then used as a masking layer for a single-step RIE pattern transfer process onto quartz substrate.

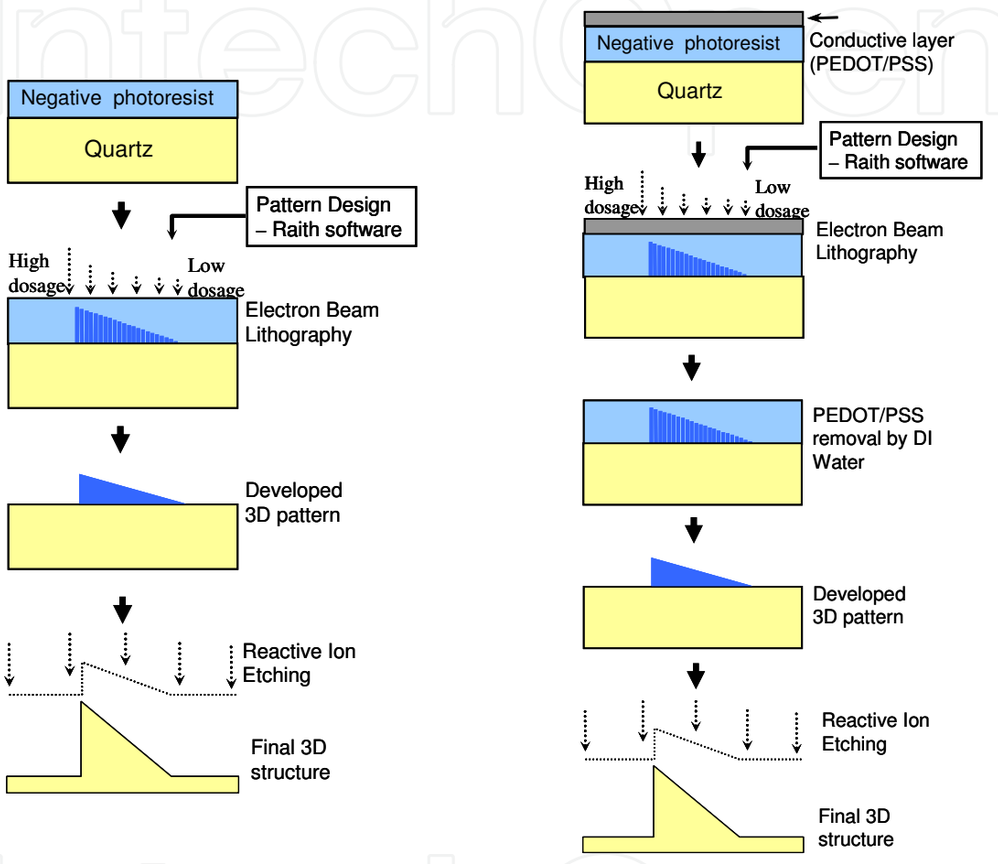

Fig. 4. Flow diagram for the fabrication process employed for 3-D structures defined on insulating substrates using (a) the critical energy method and (b) the high acceleration energy in conjunction with conductive polymer coating method.

The second approach is an application of high accelerating voltages (high energy/keV) in conjunction with the use of top conductive coatings on the resist layer. The use of high keV will produce a greater penetration depth and reduce the number of back scattered electrons which will result in a more confined beam size. Based on this approach, a Top Conductive layer method (TC) was developed and adopted in this work. In the TC method as illustrated in Figure 4(b), a water soluble conductive polymer, poly(3,4-Ethylendioxythiophene) /poly(suyrenesulfonate) or PEDOT/PSS is spun coated on the negative resist as a charge dissipation layer prior to the 3-D pattern writing. A high acceleration voltage that provides a more confined e-beam and less backscattering and proximity effects is used in exposing the 3-D pattern on a negative resist. PEDOT/PSS layer was removed by rinsing with de-ionised

water (DIW) prior to the development process. Finally the developed pattern is used as a masking layer in a single-step RIE pattern transfer process.

3.2.1 The critical energy or critical accelerating voltage

Many insulating materials often have certain charge levels where they reach equilibrium state when exposed with an e-beam. This charge equilibrium condition is reached when the charge into the sample material equals to the charge out of the sample. The charge out of the sample will be from secondary electrons (SE), backscattering electrons (BSE), Auger electrons, x-ray and whatever current is absorbed and then transmitted through the sample to the ground. This is referred to as a state of unity (Frey 2007). It can be described as in Figure 5 where the critical energy assumes a neutral charge at points E1 and E2 as suggested by J. Joo and co-workers (Joo et al. 2006). Polarity of charging is dependent on the e-beam configuration.

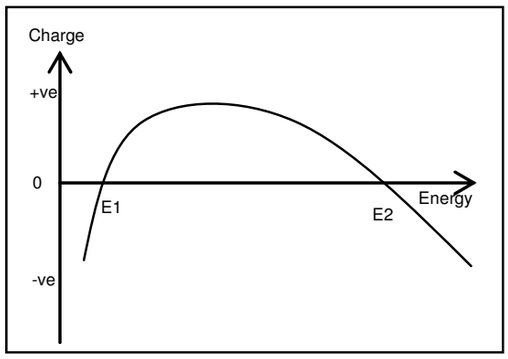

Fig. 5. The schematic diagram of the e-beam critical energy (Joo et al. 2006).

To estimate the range of suitable low energy for writing a 3-D pattern on nonconductive substrates, Monte Carlo simulation using CASINO software (CASINO Software 2006) was employed. Figure 5 illustrates the 200-electron trajectories simulation of electron beams with accelerating voltages of 4.5, 5.5, 6.5 and 20 keV. In these simulations a 600 nm thick ma-N2403 resist layer coated on a quartz substrate was assumed to be exposed by an e-beam.

The volume of electrons interaction increases when the e-beam accelerating voltage increases. At accelerating voltage of 4.5 keV as illustrated in Figure 6(a), the penetration depth of electron trajectories is far from reaching the quartz substrate surface and fully expose the resist. The volume of crosslinked negative resist after the e-beam exposure is therefore present only at the top thin layer of the exposed resist. This leads to a layer of unexposed resist close to the quartz surface and will be washed away during the developing process at a later stage.

Further simulations were carried out to find a suitable/critical accelerating voltage that will crosslink resist all the way down to the quartz surface and neutrally charge the resist. The observation from the simulation shows that high propotion of the electron trajectories settled at about 85% of the longest vertical distance. For example, as illustrated in Figure 6(b), the penetration depth of 5.5 keV accelerating voltage was estimated at approximately 550 nm which is less than the resist thickness (600 nm). At this condition, the resist surface could be negatively charged.

Simulation at an accelerating voltage of 6.5 keV as illustrated in Figure 6(c), the penetration depth is estimated at approximately 660 nm which is larger than the resist thickness of

600nm. At this condition, the resist surface could be positively charged. Based on this analysis, the critical e-beam accelerating voltage for a 600 nm thickness of ma-N2403 resist on quartz substrate is in the range of 5.5 to 6.5 keV. This method can be used as an estimation in finding the critical e-beam accelerating voltage that assumes a neutral charge for certain resist thicknesses. Accordingly, an accelerating voltage of 6.25 keV is suitable for a 600 nm resist thickness exposure. Similar approach can be followed for other resist system.

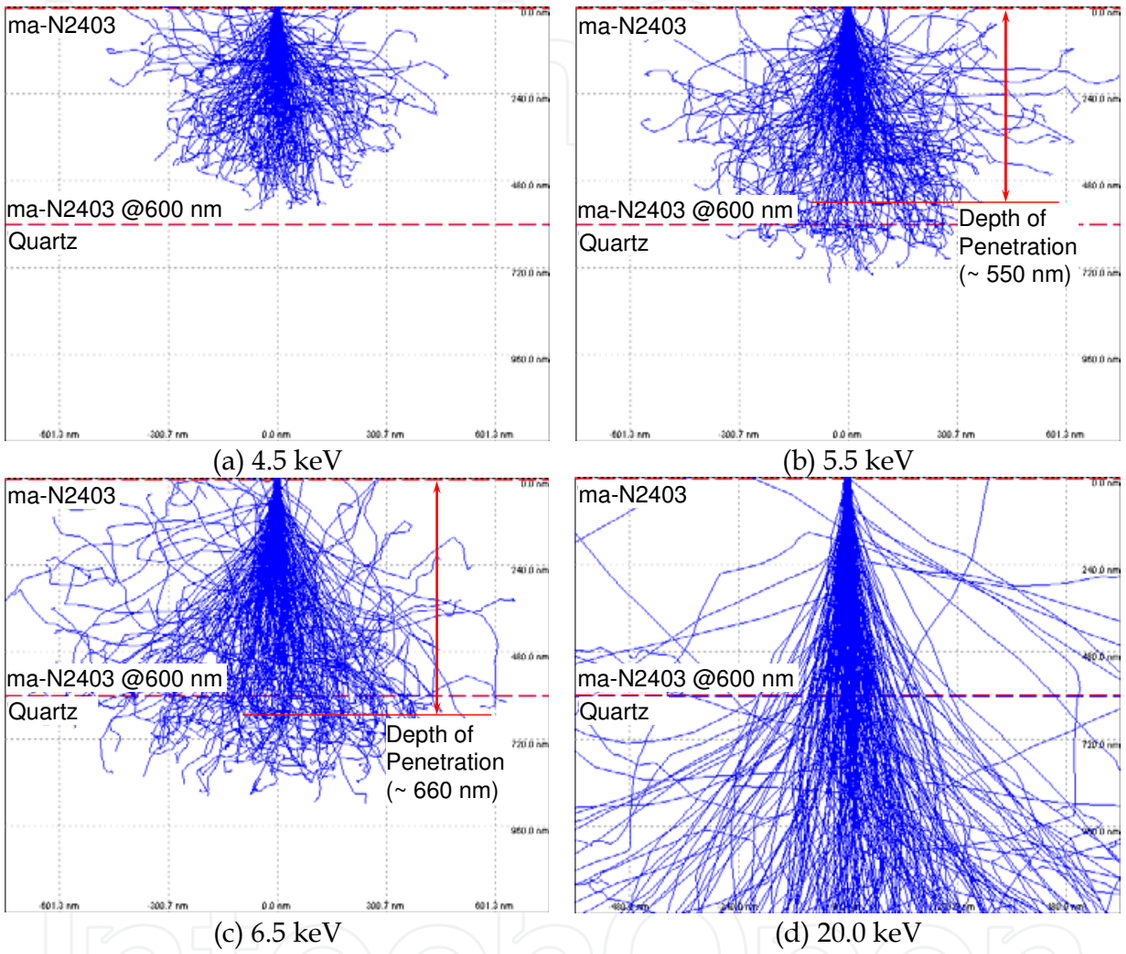

Fig. 6. Electron trajectories of various e-beam acceleration voltages across ma-N2403 resist on quartz substrate by employing Monte Carlo simulation using CASINO software.

Figure 6(d) shows the simulation of electrons trajectories when a high accelerating voltage of 20 keV is used for exposure. A very deep penetration, more confined trajectories, less electrons backscattering and less proximity effects are observed. This is useful for patterning smaller and higher density patterns which will be discussed in the next section.

Charging comes in several species often exhibiting several characteristics, either positive or negative charging. When the sample is charged positively, the image will appear dark and when there is a negative charge, the image will appear bright (Frey 2007).

Further experiments were carried out on a range of ma-N2403 resist layer thicknesses from 350 nm to 800 nm using a Raith-150 EBL tool. The actual critical energy values were determined by gradually increasing the accelerating voltage from the lowest values as

estimated by Monte Carlo simulation to the optimised level. To find an optimized or critical accelerating voltage that leaves no charging marks on the zoomed resist image under scanning electron microscopy (SEM) conditions, images obtained of resist between 200X and 500X magnifications were then zoomed in and out for each accelerating voltage increments. Figure 7 shows the critical acceleration voltage with respect to the resist thicknesses penetration that was estimated by the Monte Carlo simulations as compared to the experimental results. There were no significant differences between the two and they can be used as a guideline for e-beam exposure at any resist thicknesses.

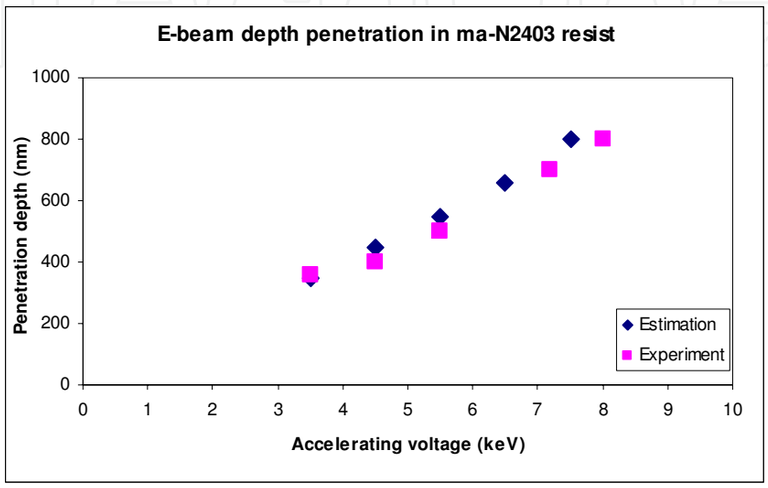

Fig. 7. A comparison of e-beam depth penetration between estimation using CASINO software and experiments, showing penetration depth increases with acceleration voltage.

As explained earlier, the e-beam voltage acceleration of 6.25 keV has been found to be the optimum to realise the minimum charging effect and therefore used for the 3-D patterning on the 600 nm thick ma-N2403 resist. The SPL pattern writing scheme was utilized for 3-D patterning with a line dosage ranging from 0.6 to 42.0 pC/cm. Examples of SPL pattern writing scheme for 3-D structures have been explained in section 3.1. After the e-beam exposure, the samples were developed in Microresist ma-D532 developer for 15 seconds at a temperature of 20 ◦C.

Figure 8(a) shows an AFM image of the developed 3-D ring structure test pattern defined on an ma-N2403 resist. This test pattern has three 3-D shaped structures. The first is the centre doom shaped lens 3 microns in diameter and 300 nm on its highest point. The second is the middle 3-D ring, which is 5 microns in inner diameter and 9 microns in outer diameter with a ramp down profile from the highest point of 300 nm at its inner diameter and zero at its outer diameter. The outmost 3-D ring structure which is 11 microns in inner diameter and 13 microns in outer diameter with a ramp down profile from the highest point of 300 nm at its inner diameter and zero at its outer diameter. This test pattern has a potential in micro Fresnel lens fabrication and other optical device applications.

Figure 8(b) shows an AFM image of the developed 3-D pyramid structures with a multilevel array test pattern defined on an ma-N2403 resist after development process. Each outer pyramid has a one micron square base and is 300 nm in height. There are four similar pyramids in the center but at an elevated level of 300 nm. The pyramid array test pattern represent what could be used as light trapping surface texturing structures for solar cells

applications. Multilevel structures are important in eliminating multistep processes and multilevel alignments reducing process complexity and lowering cost.

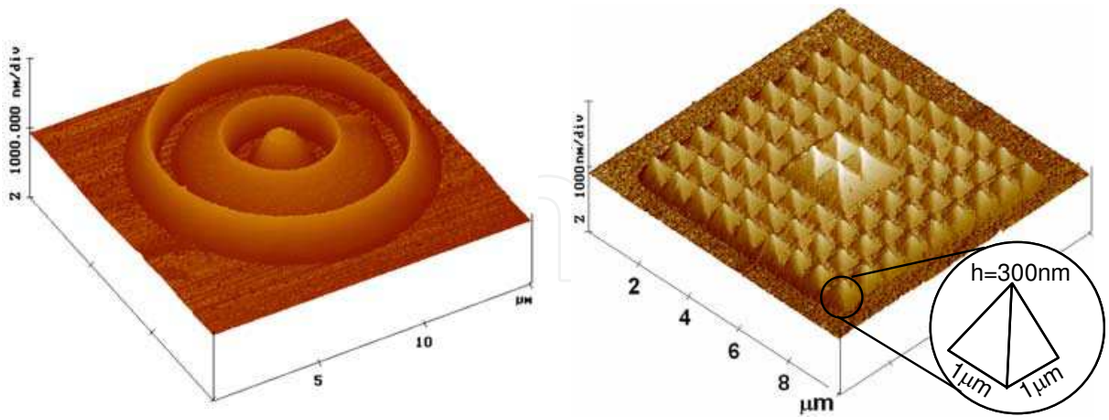

(a) (b)

Fig. 8. AFM images of the developed 3-D structures defined on ma-N2403 resist using critical energy technique (a) 3-D ring structure and (b) 3-D multilevel pyramid array.

3.2.2 Top conductive dissipation layer using PEDOT/PSS

Conducting polymers, particularly the soluble derivatives, are other potential alternatives as a charge dissipators layer for EBL pattern writing on insulating materials. We will describe in this section using a water soluble conductive polymer, PEDOT/PSS as the top conductive coating on the negative resist layer. PEDOT/PSS was spun coated on top of the ma-N2403 resist at 5000 rpm for one minute, and baked on a hot plate at a temperature of 90 ^{o}C for two minutes to achieve a thickness of about 30 nm (Mohamed et al. 2009).

The effectiveness of this material in supressing charging was verified through the exposure experiments. Figure 9 shows SEM images of quartz substrates exposed with an e-beam at a high acceleration voltage of 20 keV and with 20 μm aperture. The bottom half is an illustration of the electron trajectories penetrating the resist layer. Figure 9(a) shows an SEM image of quartz substrate coated with negative photoresist only, without the conductive polymer layer; these display the characteristic bright area of built up negative charges. No objects can be resolved for imaging or writing under the influence of surface charging. Figure 9(b) shows an SEM image of a substrate coated with negative photoresist anda top conductive coating PEDOT/PSS after it has been exposed with e-beam. No charging effects were observed at the resist surface as is evidently shown by the confined 20 nm dot where surface charging is significantly suppressed.

The surface charging build up phenomena could be explained by refering to Figure 9(c), which illustrates the schematic diagram of the electrons path that leads to secondary electron emission and built up charges by the trapped electrons. In comparison, Figure 9(d) illustrates the schematic diagram of the electrons path with the existence of a PEDOT/PSS conductive layer. Most trapped and built up electron charges are grounded through the PEDOT/PSS conductive layer.

This 3-D fabrication method was developed to overcome the limitation of the previous CE method where the creation of smaller feature below 500 nm have been hindered by electrons back scattering and proximity effects. In 3-D patterning on negative resist, the developed resist height at a particular spot is determined by the magnitude of resist crosslinking at that

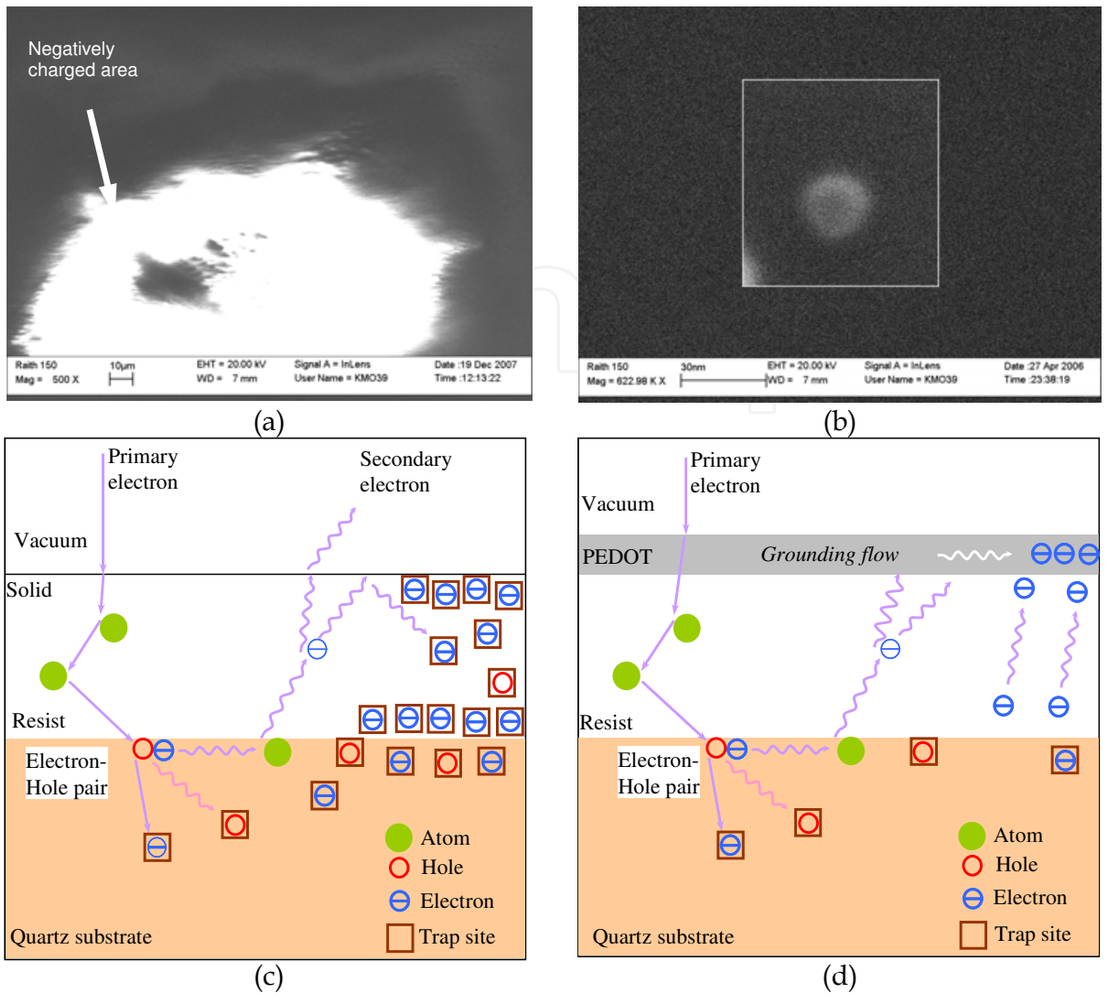

Fig. 9. A comparison between resist surfaces without and with a PEDOT/PSS conductive polymer layer. At the top, SEM micrograph of resist surface (a) without charge dissipator layer showing bright area (negatively charged) and (b) with charge dissipator layer of PEDOT/PSS. At the bottom, schematic diagrams showing possible electron trajectories for resist exposed to e-beam. (c) electron trajectories without the charge dissipator layer and (d) with the charge dissipator layer.

location due to direct e-beam exposure plus the proximity effects from adjacent exposures. At lower voltage acceleration of below 10 keV, the spread of the e-beam is quite large (up to 3 μm) as referred to Figure 5. Hence, the developed resist height at a particular spot is heavily affected by multiple electrons' backscattering and proximity effects caused by line exposures near to the spot. Exposing a line with low dosage does not necessarily produce a lower resist height if the surrounding lines are exposed with high dosages. Manual optimisation of line dosages in order to achieve certain resist height in 3-D patterning requires a long iteration experiment process owing to multiple electrons' scattering and proximity effects from surrounding exposures.

In the following method, a higher voltage acceleration of 20 keV has been employed as compared to 6.5 keV used in previous method that followed the CE method. The single pass

line (SPL) pattern writing scheme was utilized for 3-D patterning with line dosages starting at 0.6 pC/cm up to 42.0 pC/cm. Figure 10(a) shows an example of a 3-D pattern writing scheme for a 300 x 300 nm² base pyramid. It was created using e-beam writing on the negative resist by routing the multiple SPL parallel paths with various dosages assigned for each SPL (path 1 to path 6). The spaces between each SPL route ranged from 20 nm to 30 nm. Figure 10(b) shows an AFM image of the developed 3-D pyramid test pattern on a ma-N2403 resist. Each pyramid has a 300 x 300 nm² base and is 300 nm in height.

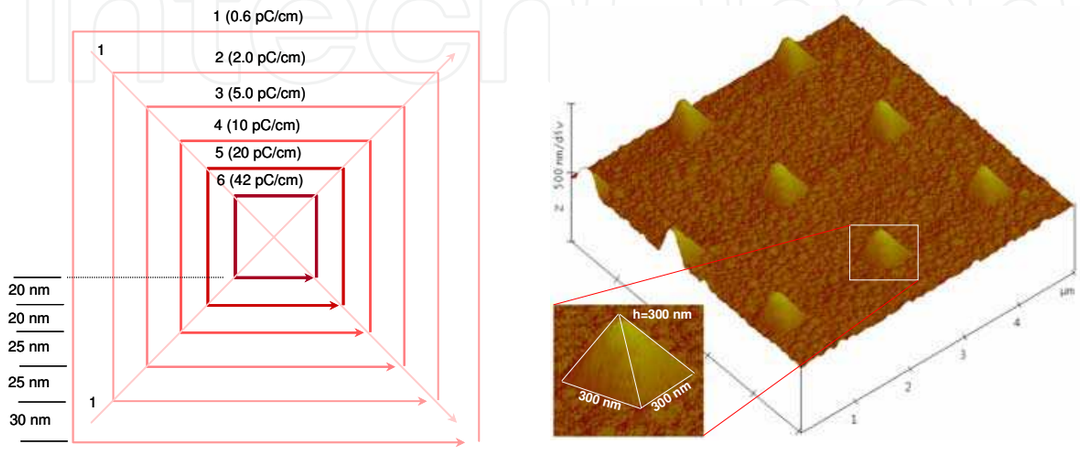

(a) (b)

Fig. 10. EBL writing scheme for 3-D patterns (a) SPL routing for writing a 300 x 300 nm² pyramid and (b) AFM image of the exposed and developed 300 x 300 nm² pyramid array.

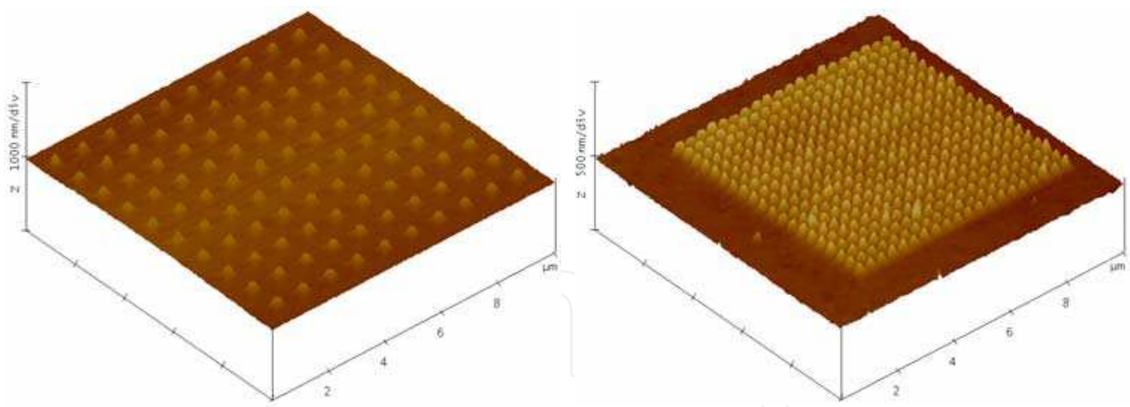

(a) (b)

Fig. 11. Maximum pattern density achieved using the two pattern writing methods (a) critical energy method and (b) top conductive coating method, where much higher densities are evident.

The advantage of exposing an e-beam at a higher acceleration voltage is the minimisation of electrons' scattering and lowering of proximity effects on the surrounding exposed region as illustrated by confined electron trajectories as shown in Figure 6(d). This results in a better control over the developed profiles, less time required for the dosage optimization process, and the achievement of higher pattern density of 3-D patterns is possible. Figure 11(a)

shows an AFM image of an array of a 500 x 500 nm² pyramid structure with 800 nm pitches. These are the maximum density pitches achieved using the previous pattern writing method where low accelerating voltage of 6.25 keV is used. In this example the electrons backscattering and proximity effects have limited the density 3-D structures. Figure 11(b) shows an AFM image of an array of cone structure (300 nm base diameter) with 400 nm pitches which were achieved using a TC pattern writing method. A much higher density 3-D pattern is possible with the proximity effects suppression using a combination of higher accelerating voltages and top conductive coating. This high accelerating voltage allows deeper penetration, more confined beam, and less electrons backscattering and proximity effects.

3.3 Pattern transfer

The developed 3-D patterns have been directly transferred into the quartz substrate by a single-step RIE with suitable selectivity of resist-to-substrate by optimising the etching process parameter. CHF_3/Ar gases were chosen for quartz etching based on their moderate F/C ratio which is important in the 3-D pattern transfer.

RIE Parameter	Setting/measured
Gas	CHF_3/Ar
Flow rate	9.0/6.25 sccm
Pressure	< 6 mTorr
Temperature	295 K
RF Power	125 W on 100 mm electrode
Bias voltage	-344 V
Selectivity resist-to-substrate	1:2
Etch rate	10 nm/min on quartz

Table 1. The optimized CHF_3/Ar RIE parameter for 3-D pattern transfer onto quartz substrate.

We will describe here how to achieve a smooth linear gradient or curved 3-D surface profiles of the fabricated mold with a surface roughness of less than 5 nm after the RIE pattern transfer process. This is an essential requirement for micro optical devices where the general guidelines required the surface roughness have an upper limit of 5 nm.

It is a challenging task to create a relatively tall 3-D structure using the EBL 3-D patterning technique owing to the electrons back scattering and proximity effects even with charge suppression approaches. Hence, an upper limit of 600 nm is imposed on the 3-D structures in this case. This aspect ratio has been achieved through appropriate resist to substrate selectivity. The RIE pattern transfer parameters were optimised to yield 1:2 resist-to-substrate selectivity ratio which is suitable for transferring the 3-D pattern on quartz. Table 1 shows the final optimized RIE parameter employed to achieve a smooth surface finish with surface roughness of less than 5 nm and 1:2 selectivity.

3.4 Etching analysis

Plasma discharges involves quite complex mechanisms and can be difficult to interpret or even understand in some cases. In fluorine–containing plasma for example, surface reaction, etching, and polymerization can occur at the same time. The domination of certain reactions

is dependent on the gas feed, the operating parameters and the chemical nature of the polymer/substrate, electrode and geometry (Chan et al. 1996). In a quartz etching process using CHF_3 etchant, the free fluorine radicals, F* are created by the plasma discharge and the etching chemistries can be described as follows;

$$e^- + CHF_3 \rightarrow CHF_2^+ + F^* + \text{radicals} + 2\,e^- \quad (1)$$

$$SiO_2 + xF^* \rightarrow SiF_x + O_2 \quad (2)$$

$$CF_x \text{ radicals} + 2O_2 \rightarrow CO + CO_2 + COF_2 \quad (3)$$

F* is the reactive fluorine atom and SiO_2 is the quartz substrate. RIE plasma generates reactive fluorine atom F* from the supplied CHF_3 gas (Eqn 1). The etching of quartz consumes the F atom to form a SiF_x (Eqn 2). One of the radicals, the CF_x radicals, tend to deposit polymer films on all surfaces under certain condition, but the oxygen liberated in the etching of quartz reacts with CF_x radicals to form volatile CO, CO_2, and COF_2 (Eqn 3). In 3-D pattern transfer, the presence of resist which is polymer based acting as the 3-D masking layer, will increase the C content. The backbone of resist polymer consists of $C_xH_yO_z$ elements which react with plasma gases, creating the volatiles of these elements. This process decreases the F/C ratio, causing domination of polymerization reactions, in other word deposition instead of etching. Figure 12 illustrates the 3-D etching chemistry analysis. The reactive ions bombarding the 3-D surface in a vertical downwards direction, irrespective of the resist pattern shape of profile.

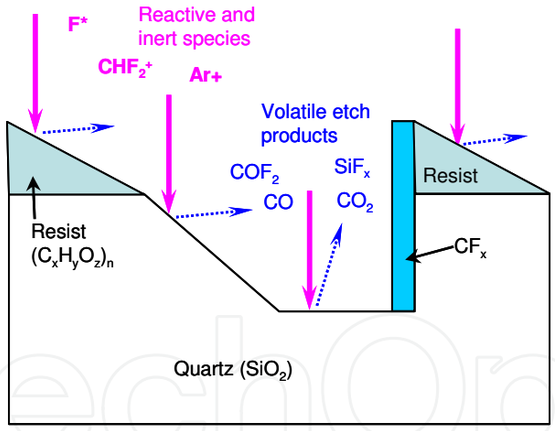

Fig. 12. The schematic of 3-D etching chemistry, showing the fluorinated reactive gases and the by-products during etching quartz.

Let us consider a plasma etching on an inclined quartz surface at an angle θ where the plasma bombardments are most likely to occur in a vertical downwards direction as illustrated in Figure 13(a). Ion bombardments on the ramped surface will bounce/backscatter in a downhill direction. The bounced ions from the inclined substrate surface collided with the incoming ions from the top causing another bouncing down the slope.. Cumulatively, the plasma concentration will increase towards the downhill direction. Higher plasma concentration induced a higher etch rate (about 10 nm/min) as illustrated in Figure 13(b). The steeper the surface slope is the higher and the narrower the plasma

concentration at the bottom of the slope at location D. Moreover, during resist etching, the ion/resist ratio at the thin resist side caused a higher etching rate on the thin resist layer as compared to the thick resist layer. As for the 3-D masking layer, the different resist masking thicknesses will cause a varied etching rate on every location.

Backscattered and bounced ions towards the vertical or sloped walls will collid with the vertically incident ions creating a higher concentration of ion bombardment at the bottom of the structures, thus causing a trenching effect as illustrated in Figure 13(c). At location C, the trenching effects result in a wider channel as compared to the narrow trench observed at location D. Location D represents the trenching effect of an inclined surface when the inclined angle θ is approaching 90^{o}.

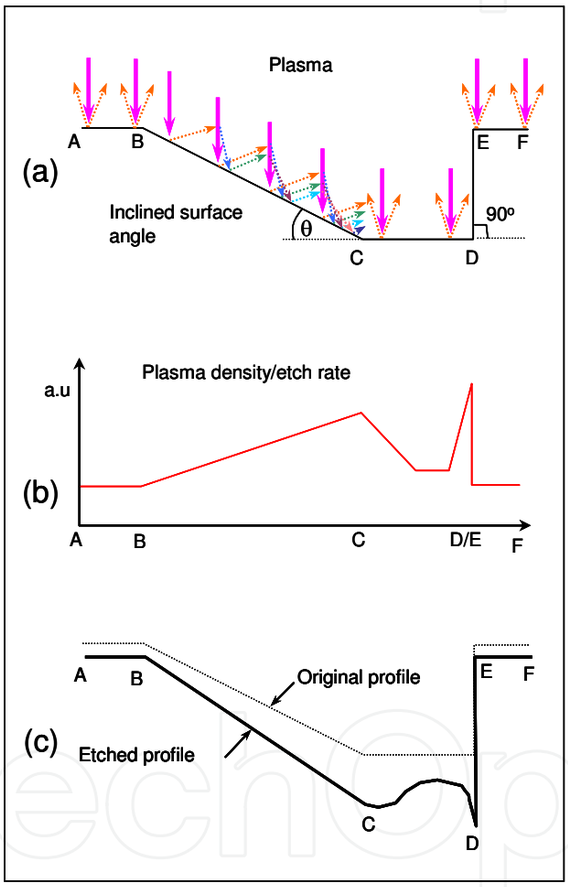

Fig. 13. The 3-D etching mechanism showing the trenching effects at the bottom of the structure.

Figure 14(a) shows an SEM image of the centre of the 3-D ring shape on quartz after the CHF_3/Ar RIE process. It shows the final 3-D ring etched profile with the lens shape in the middle and the vertical sidewall profile for outer ring. The trenching effects formed around the 3-D lens and at the bottom of the sloped 3-D ring structure are observed. Figure 14(b) shows the AFM cross sectional traces of the 3-D ring mold structure with trenching effects. Due to the deep trench profiles it is not possible to trace perfectly the actual topography owing to the limitation of the AFM tip itself.

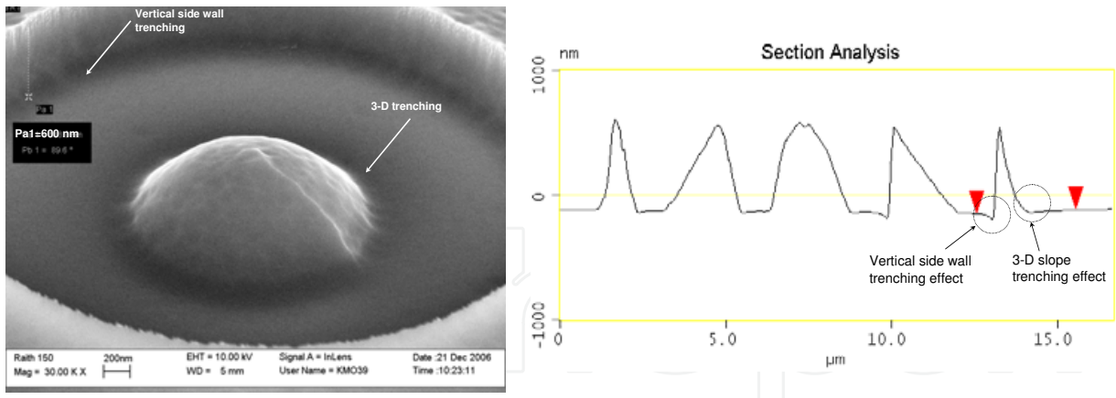

(a) (b)

Fig. 14. Trenching effects (a) SEM image of the central dome shaped lens and the 3-D ring etched profile and (b) AFM traces of cross section into the structure.

In etching hard materials such as quartz where polymerization reactions dominate, high plasma density is essential to increase the etching rate, especially for a deep etching in a 3-D pattern transfer process. High plasma density can be achieved by increasing the RF power and/or reducing the electrode surface area (loading effect). The maximum RF power that can be set on an Oxford Plasma 80plus RIE is 200 Watts. In this experiment, a NiCr coated electrode was clamped with a two-inch (50 mm diameter) PTFE electrode holder. Hence, the maximum plasma density is set to the highest setting of 10.2 W/cm^2 with this arrangement. In this high density etching process where polymerization reactions dominate, some of the etched materials may drop/deposite back on the sample forming a nanomasking island. This will form nanopillars as illustrated in Figure 16 and will be discussed later.

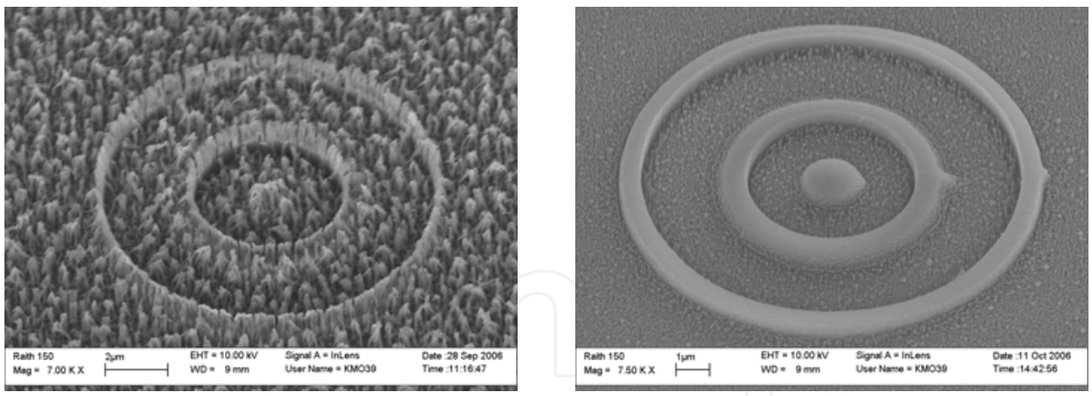

(a) (b)

Fig. 15. SEM images of the etched 3-D structure on quartz substrate. (a) and (b)

The highly dense nanopillar structures that formed as a result of the plasma etching process will finally collapsed after high density plasma bombardment over a long period of time. Figure 15(a) shows an SEM image of a 3-D ring structure when etched with the high density plasma setting of 10.2 W/cm^2 for 40 minutes. The result shows a very rough surface and a vertical sidewall passivation layer can be clearly observed. It can be concluded that increasing the plasma and/or power densities above certain levels to achieve high etching rates would not achieve a smooth etched surface as desiredfor the 3-D patterns used for optical devices or for UVNIL molds.

In the following experiment, the plasma density was reduced to a normal condition by changing the electrode area (by changing the size of the clamp ring) to the 100 mm diameter electrode holder which gives a plasma density of 2.5 Watts/cm^2 with RF power of 200 W. It is found that the surface roughness is improving by lowering the RF power density as shown in Figure 15(b).

Since this etching process was dominated by polymerization reactions, CF_x radicals tended to be deposited anywhere on the etched surface. At an operating pressure of 20 to 30 mTorr, the mean free path of the plasma species is very short (less than the distance between the sample and the RIE anode of about 120 mm) and etching species are in close proximity to each other causing continuous collisions. In this saturated condition, the species produced as a result of ion bombardment of the resist mask material and substrate surface will reach a level at which the vacuum pump is unable to extract away these by-products. The lack of vacuum pumping capacity will lead to dropping of the etching products and particles back onto the substrate surface causing nanomasking effects as illustrated in Figure 16(a) and (b). From the above experiments, it was found that the etching process was limited by the vacuum pumping capacity in extracting the etching by-products during the etching process at this condition. The micro/nanomasking effects in conjunction with polymerisation under certain CHF3 plasma conditions have resulted in the formation of the nanopillars shown in Figure 16. These nanopillars are 30-50 nm in diameter and about 500 nm tall.

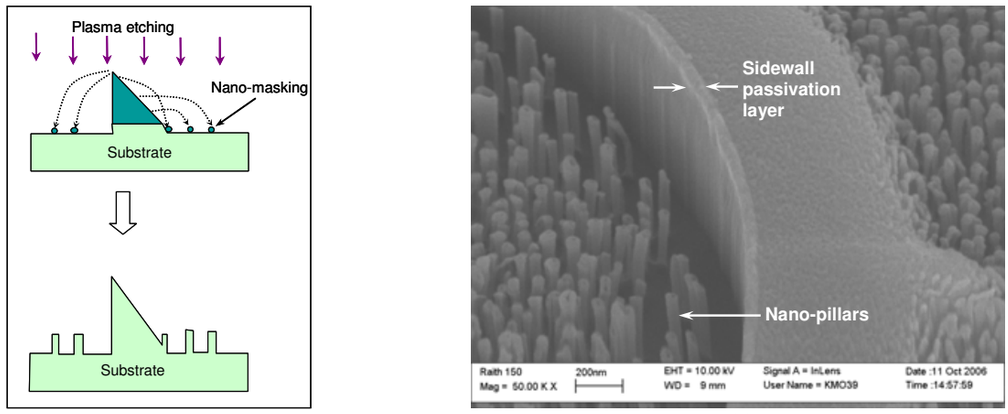

(a) (b)

Fig. 16. (a) Illustration of the possibility of how the pillars are formed through nanomasking effect (b) SEM image of quartz showing the nanopillars and sidewall passivation layer.

To achieve a smooth surface finish, an etching process with a moderate plasma density and a higher physical than chemical reaction should be followed. The optimum etching process should be then set at below the maximum capacity of the vacuum pumping. In that sense, a very low operating pressure is required so that the etching products are extracted immediately before they are allowed to drop on the sample surface. This process is similar to the physical etching mechanism. At a very low operating pressure condition below 20 mTorr, the mean free path is increased, which minimizes the collision between atoms and ions. To achieve low operating pressure, the gas feeds have to be reduced. As a result, the products of the chemical reaction are largely minimized and the etching is mostly carried out by the physical bombardment. This condition was achieved by reducing the incoming flow rates of the etching gases which results in a lower operating pressure but also lower etching rate.

From the above experimental analysis, it was found that the operating pressure has a direct effect on the surface roughness. Further experiment has demonstrated the relationship between the surface roughness and etching pressure as illustrated in Figure 17. The AFM was used to measure the surface roughness of the etched samples. A surface roughness of about 85 nm is measured when the etching pressure is 30 mTorr. At 25 mTorr processing pressure, the measured surface roughness was much lower than actual because of the limitation of the AFM in tracing the nanopillars effectively. A lowest surface roughness $R_{q(rms)}$ of 1.429 nm was measured at etching pressure of below 6 mTorr.

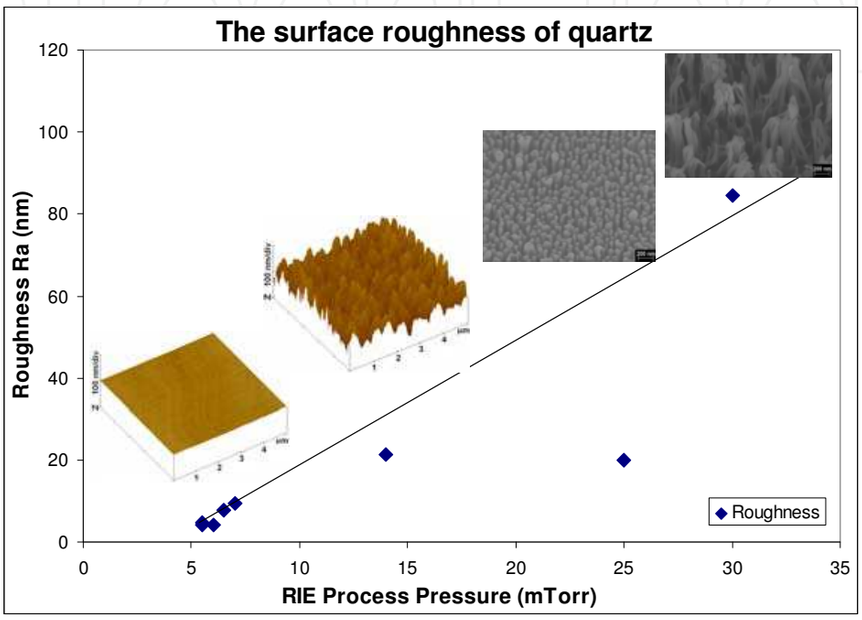

Fig. 17. The surface roughness versus the RIE operating pressure. The upper two SEM images represent high pressure process with high level of roughness, while the bottom AFM images showing very smooth surface obtained by low RIE process pressure.

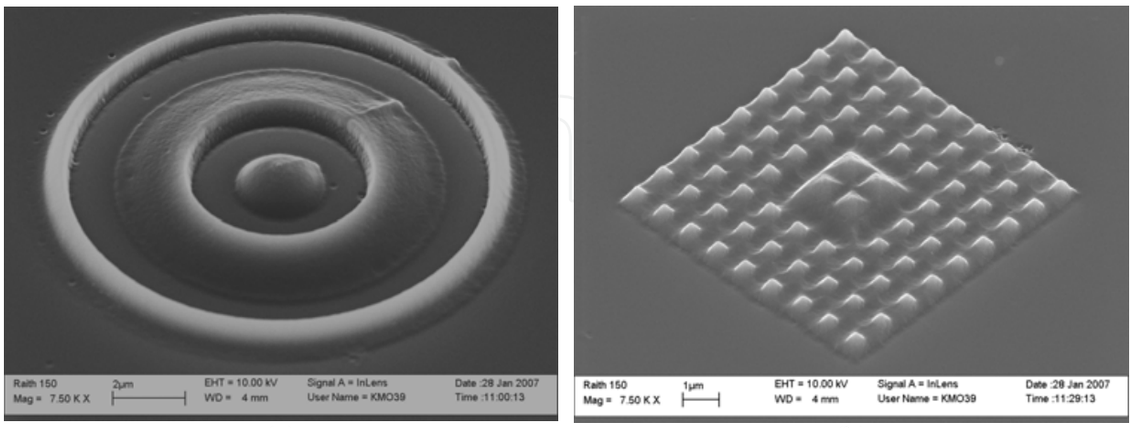

(a) (b)

Fig. 18. SEM images of the etched 3-D structures on quartz substrate (a) 3-D ring and (b) 3-D multilevel pyramid array. The 3-D structures shown are used as the master molds in the subsequent imprint process.

Figure 18(a) shows an SEM image of the 3-D ring structure on a quartz master mold substrate with the highest point on the pattern of 600nm. Figure 18(b) shows an SEM image of 3-D pyramid structures with multilevel features on quartz substrate. These structures were used as the test pattern for the master mold in the 3-D nanoimprint lithography.

4. Imprints

Imprint is primarily a physical deformation process where a mold with micro/nanostructures on its surface is utilized to deform a thin resist film (or an active material) deposited on a substrate (Chou 2003). The resist can be either a thermal plastic or UV curable material. It is a direct pattern transfer technology where the resolution is independent on light wavelength or electron scattering. A wide range of substrates and mold materials are possible. Quartz, SiO2, Si3N4, and Ni are typical molds used in NIL. NIL is a low cost, high throughput technique suitable for patterning micro and nanostructure. Another unique feature of NIL technology is that it is a direct 3-D patterning technology, which is not achievable in other lithography technologies.

There has been a strong demand imposed by semiconductor industries for an innovative lithography technique, where nano-scale resolution, high throughput and cost-effectiveness are fused together, and the NIL technologies can satisfy these criteria.

In the imprint experiments, a simple vacuum operated manual imprint tool was attached onto the UV exposure stage of the Karl Suss Mask Aligner system. An UV illumination of 365 nm wavelength with an intensity of about 0.6 W/cm^2 was utilized for resist curing while imprinting. In imprinting, achieving the thinnest possible residual resist layer is an essential requirement to ensure a successful pattern transfer. This requires optimization of pattern density, resist viscosity, resist thickness and imprint pressure. Hence, the study of the behaviour of resist reflow during and after imprint is important in NIL technologies (Macintyre & Thoms 2005; Mohamed et al. 2006) .

In this section, imprint problems such as sticking, air bubbles, and the uniformity of the residual resist layer will be discussed. For sticking issues, a number of options were followed in order to modify the mold substrate surface properties such that surface chemistry for each material used was considered to minimize the sticking problems. Surface treatment of polymer using plasma to modify the surface energy is a common technique and has been studied extensively with wide range of suggestions and solutions (Chan et al. 1996). Minimization of defect density and contamination are also important aspect in imprinting processes. This is considered one of the limitations of current NIL technique.

De-molding is the process by which the mold is separated from the imprinted polymer structure by a vertical movement of the mold. This is a crucial step in the imprint process and extra care must be taken to minimize failures at this stage. Distortion or damaging of the imprinted structure during this movement can happen as a result of different effects such as adhesion of resist at the surface, friction due to surface roughness of sidewalls and trapping of the polymer due to negative slope of cavity sidewalls. De-molding without resist damage is one of the key elements for successful nanopatterning using NIL technology. Some demolding examples by separating the mold and substrate using an air knife has been demonstrated by S. Merino and co-workers (Merino et al. 2007).

In 3-D imprinting, the pattern on the mold has to be the inverted shape of the intended 3-D structure. The mold making process of the inverted shape of the intended 3-D structure can be quite difficult. Hence, an imprint technique was used to replicate the inverse shape of the

mold from the master mold. This process is similar to a casting or moulding process widely used by the manufacturing industry. It allows the master mold structures to be fabricated on any material and later replicated on the intended materials.

4.1 Imprint preparation

In the 3-D imprint, an Ormocomp resist from Microresist Technology was used as the imaging layer for the first imprint step and a mr-UVCur06 resist from Microresist Technology was used in the second imprint step. Ormocomp has excellent properties for UV transmission which is crucial as a transparent mold, while mr-UVCur06 has low viscosity which is essential to achieve a minimum and uniform residual resist thickness in Imprint 2 step. Therefore two steps imprint is usually followed.

The required resist thickness for Imprint 1 is dependent on the height of the master mold structure and the pattern density. The resist should not be too thick compared to features on the mold to avoid the shrinkage stress during the UV curing process because of a high stress is normally present at the edge of the 3-D patterns. A 400 nm resist thickness is found appropriate in replicating the 3-D master mold. To achieve this thin layer, a 30% Ormocomp diluted in Ormothin solution was spun coated on a quartz substrate at a spinning speed of 3000 rpm for one minute and pre baked on a hot plate at 80^{o}C for two minutes (Mohamed et al. 2008).

For imprint 2, the required initial resist thickness is more critical as it determine achieving a minimum residual resist thickness. A 400 nm thick of mr-UVCur06 resist was found appropriate to yield a residual resist thickness below 100 nm. The resist was spun coated at 2800 rpm for 45 seconds and pre baked on a hot plate at a temperature of 80 ^{o}C for two minutes to achieve a 400 nm resist thickness.

Prior to the UV resist coating, quartz substrate was cleaned and surface treated using oxygen plasma to promote better adhesion at the interface between quartz and resist surface. It is important ensuring that surfaces in contact during the imprint process have low surface energies to minimize the sticking problems. Surface wetting experiments were carried out to identify the wetability of the surfaces involved in the UV-NIL imprint process. Figure 19 shows the contact angle of different materials in a normal condition and after

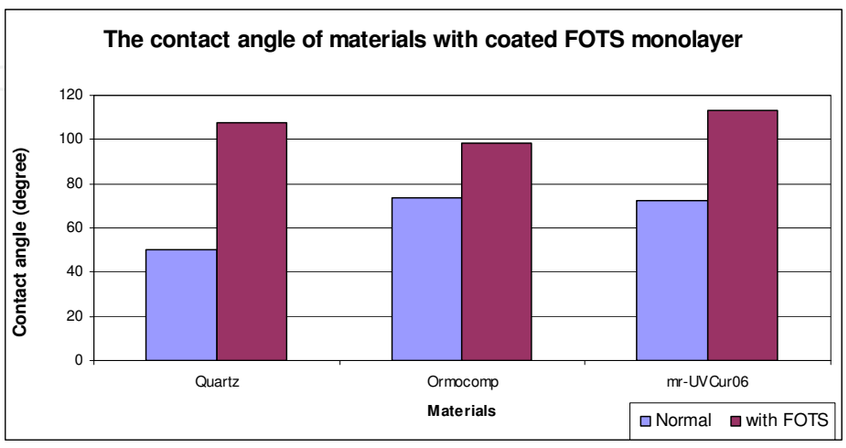

Fig. 19. The contact angle measurement of the imprint materials in normal condition and after being coated with a FOTS anti adhesive monolayer.

being coated with a 1H, 1H,2H,2H-Perfluoroocty-trichlorosilane (FOTS) anti-adhesive monolayer. Another method of minimising the sticking problem is by surface treatment using plasma. A contact angle up to 80^o can be achieved on quartz or silicon substrates when exposed to SF_6:CHF_3 1:1 plasma (Sun et al. 2008). The resist surface can also be treated using fluoride containing plasma such as CHF_3 (Chan et al. 1996) in order to increase the contact angle. Table 2 shows the RIE recipes for the surface treatments of quartz and resist.

	Quartz surface	Resist surface
Gases	SF_6 / CHF_3	CHF_3
Flow rate (sccm)	15.0/15.0	30.0
Pressure (mTorr)	28	30
Temperature (K)	295	295
RF Power (W)	50	100
Time (s)	120	30
Max. contact angle	Up to 80^o	Up to 85^o

Table 2. The RIE parameter for surface treatment employed in minimising the sticking problem and in achieving the desired contact angles.

4.2 Imprint processes

The manual vacuum operated imprint tool was used in this imprint experiment to create a vacuum environment in order to reduce the air bubbles trapped in between the mold and the resist during the imprint process.

Replicating the 3-D structure of the master mold involved two imprint steps. The first imprint (Imprint 1) replicates the inverted shape of the master mold while the second imprint (Imprint 2) replicates the inverted shape of the first imprint (Imprint 1) which became the positive replica of the original master mold.

Two 3-D test master molds were used in this work, the first was the 3-D rings structures (Figure 17(a)) and the other was the 3-D multilevel pyramid structures (Figure 17(b)). A very thin monolayer of FOTS was used as an anti sticking layer on the quartz mold surface. It was deposited on a mold surface by a natural convection method in a petri dish at room temperature.

In this work, the filling of the 3-D cavities with the resist and the required initial resist thickness were investigated by a trial and error method but guided by simulation of resist reflow behaviour (Mohamed 2005). The 100 % cavity filling in the 3-D mold, the required imprint pressure and minimum residual resist thickness were optimized accordingly.

4.2.1 Imprint 1

The purpose of the first imprint was to replicate the inverted shape of the master mold onto a UV curable resist. Figure 20 illustrates the schematic diagram of the Imprint 1 process step. The 3-D mold was placed face up at the bottom of the imprint tool to ease the release of trapped air bubbles from the mold structures. The 400 nm thick Ormocomp resist coated on the quartz substrate with the face down was manually aligned on top of the 3-D master mold. The vacuum pressure of the mask aligner MA-6 which was set at 4 mbar was then activated and followed by UV flood exposure at a room temperature. Under 365 nm UV illumination, Ormocomp resist requires 300 mJ/cm^2 energy for curing, which is about an 8 minute exposure time using 0.6 mW/cm^2 illumination intensity.

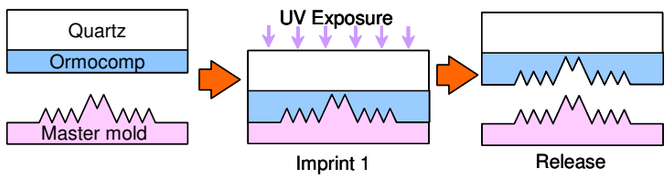

Fig. 20. The process flow of the first imprint step (Imprint 1), showing the master mold and quartz substrate coated resist exposed to Uv light and then separated.

Figure 21(a) shows a close-up AFM image of the associated imprint results of the 3-D ring mold that was made in section 3.3 and 3.4. The master mold profile was faithfully replicated. Figure 21(b) shows the AFM image of the imprint results of the 3-D multilevel molds. In AFM, a STING tip from Mikromash was used to trace the profiles of the 3-D imprint cavities.

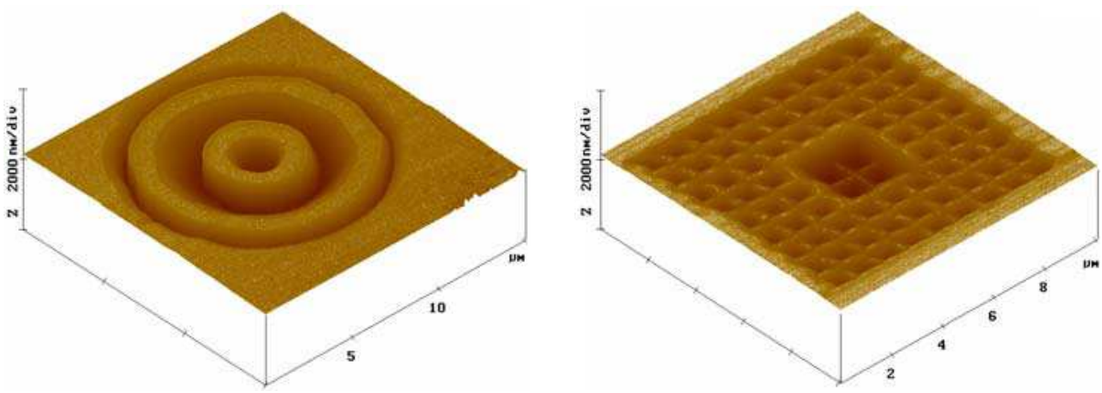

(a) (b)

Fig. 21. The AFM images of the replication of 3-D structures (a) 3-D ring and (b) multilevel pyramid, on Ormocomp resist after Imprint 1 process.

The soft mold requires a material which is durable and robustfor a successful repetitive imprint process, it should be solvent resistant and can withstand a long UV exposure. Therefore, the Ormocomp resist was hard baked at 185 ^{o}C for 2 hours to improve its hardness and enhance its solvent resistance properties.

4.2.2 Imprint 2

The purpose of the second imprint is to replicate the inverted shape of the master mold onto another UV curable resist layer in order to produce the replica of the original 3-D structure. Figure 22 shows the schematic diagram of Imprint 2 process steps.

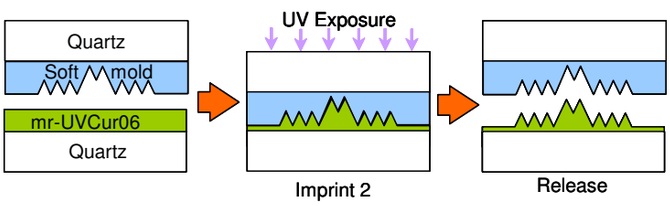

Fig. 22. The process flow diagram of the second imprint step (Imprint 2) to produce the positive replica of original pattern.

The relationship between the resist reflow and cavity filling versus the initial resist thickness is important to understand. To achieve a minimum residual resist thickness, a specially formulated mr-UVCur06 resist which has low viscosity was used. With proper optimisation, a 10 nm thick residual resist layer could be achieved. For Imprint 2 process, the 365 nm UV source was used to expose the samples for 2 minutes at room temperature. A post imprint bake at a temperature of 120 ^{o}C on a hot plate for 5 minutes to make it harder as masking layer against RIE was carried out after the sample was released from the soft mold. Imprint 2 results were imaged using the AFM technique as it does not require deposition of anti-charginglayer as in SEM. Figure 23(a) shows AFM image of the positive replica of the imprinted 3-D ring structure. Figure 23(b)} shows the AFM image of the imprinted 3-D multilevel structure on the mr-UVCur06 resist. It can be observed that the pattern has lost some of its original sharpness during the de-molding process.

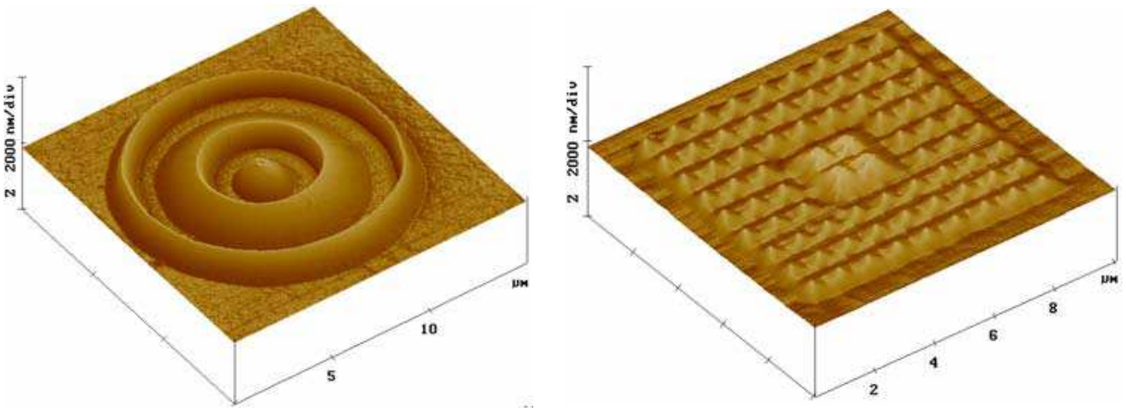

(a) (b)

Fig. 23. The AFM images of the replication of 3-D structures (a) 3-D ring and (b) multilevel pyramid, on mr-UVCur06 resist after the Imprint 2 process. The pattern in (b) has lost some of its sharpness due to de-molding.

4.3 The 3-D imprint analysis

To test the reproducibility of patterns and mold resilience against repetitive use, the imprint process was performed for 35 cycles. The results showed that by using anti-adhesive layer of FOTS coated on the quartz mold surface in Imprint 1 process, faithful replications was achieved without any deterioration of mold or resist pattern. On the other hand it was found that only 5 imprint cycles were successful without the FOTS. In the Imprint 2 process, up to 26 cycles were achieved with the FOTS coating on the soft mold (Ormocomp), however, only 3 imprint cycles were successful without FOTS coating. Imprint failures are mostly due to sticking of residual resist on the mold or as a result of particles contamination present on the mold or on the substrate.

One of the shortcomings of the Ormocomp resist is that it becomes brittle after a long UV exposure. The material brittleness combined with stress cycles in the imprint process make the Ormocomp soft mold easily to crack after about 5 imprint cycles. Micro-cracks on the soft mold surface will limit the repetition of the imprint cycles. A 5 nm of sputtered TiO_2 layer was coated on the soft mold surface as a permanent anti-sticking layer as well as to improve the hardness of the mold surface. The mold surface cleanliness will also be improved resulting in increased 15 repetitive imprint cycles. Cracks in the soft mold were

observed only after 15 imprint cycles, which caused the resist to stick to the mold surface. Figure 24(a) shows the sticking problem of the imprinted 3-D ring structure on the Ormocomp resist during the Imprint 1 process. Figure 24(b) shows a similar sticking problem of the imprinted 3-D multilevel structures on the Ormocomp resist.
The imprint pressure must always be at a low level (below 100 mbar) to avoid such sticking issues, soft mold breakage as well as maintaining the cleanliness.
In imprint 2, the problem of a low viscosity (14 mPa s) of the mr-UVCur06 resist has resulted in resist penetration into mold cracks and microcavities causing sticking issues and mold breakages at high stress points. Other than using a release agent as an anti-sticking layer, the sticking problem can also be minimized by resist surface treatment to change the surface properties.

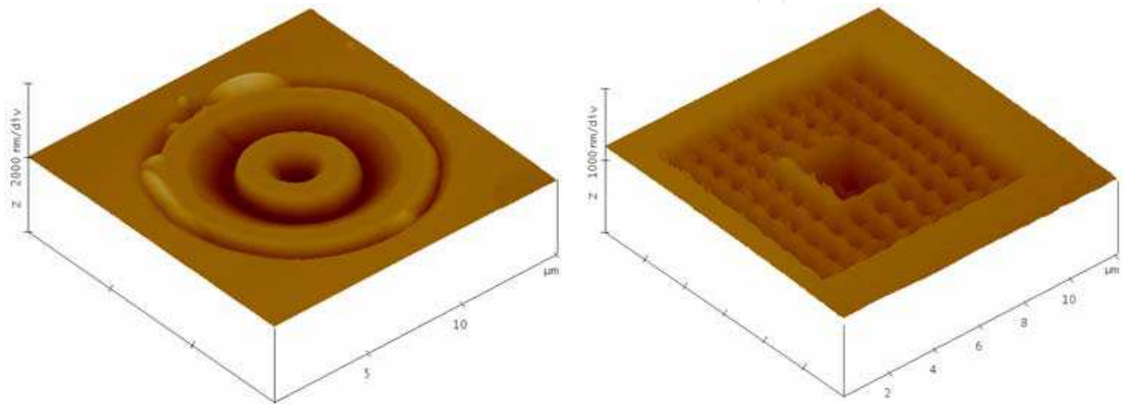

(a) (b)

Fig. 24. Examples of sticking problem of 3-D imprinted structure using Ormocomp resist, (a) sticking on the outer ring of 3-D ring structure and (b) sticking on the multilevel structure.

5. Conclusions

Direct three-dimensional patterning is demonstrated using UV cured nanoimprint lithography (UVNIL). The 3-D mold profiles were created on the ma-N2403 negative tone photoresist using the Raith-150 EBL tool with variable dose controlled exposure. A variable e-beam dose was used to obtain a resist contrast curve to determine the gradient of various 3-D structures. For a 600 nm layer thickness of ma-N2403 resist, the e-beam critical energy was set at 6.25 keV. To suppress charging effects on insulating substrate such as quartz, a conductive polymer layer is used. A higher acceleration voltage of 20 keV was used for the conductive polymer (PEDOT/PSS) top coating is employed. The variable EBL exposure with line dosages ranging from 0.6 pC/cm to 42.0 pC/cm were used for 3-D resist contrast approach. A linear resist contrast profile was obtained with a negative tone photoresist and subsequently was utilized as the 3-D masking layer. The 3-D pattern was transferred onto the quartz mold substrate by an optimized single-step reactive ion etching (RIE) process with selectivity resist-to-substrate of 1:2 using fluorinated plasma CHF_3/Ar.
The main challenging issues in EBL writing on insulating substrates are surface charging, electrons backscattering and proximity effects. The use of critical acceleration voltage and high accelerating voltage in conjunction with conductive polymer PEDOT/PSS have

suppressed the surface charging effects in the fabrication of 3-D structures, where feature size down to 300 nm has been demonstrated using this approach.
The high surface roughness caused by nanomasking and polymerisation effects in the 3-D etching process is the combined result of plasma bombardment/collision products, etched masking particles and dominating polymerization reactions at a high operating pressure. By working at low RIE operating pressure a smooth equartz surface is produced. A surface roughness of below 2 nm was achieved when the RIE process pressure was lower than 6 mTorr. In 3-D imprinting two imprint steps are involved. A 400 nm thick Orcmocomp and mr-UVCur06 resists were used in Imprint 1 and Imprint 2 processes respectively. A 3-D ring with a height of 600 nm and a multilevel pyramid array with each pyramid dimension of one micron square base and 600 nm in height were replicated. Complex three-dimensional and multilevel nanostructures can be reproduced faithfully using UVNIL, this demonstrate the potential of NIL in nanoscale device fabrication.

6. References

CASINO Software. (2006). "Monte Carlo Simulation ".

Chan, C. M., Ko, T. M., and Hiraoka, H. (1996). "Polymer surface modification by plasmas and photons." *Surface Science Reports*, 24(1-2), 1-54.

Chiu, W. L., Alkaisi, M. M., Kumaravelu, G., Blaikie, R. J., Reeves, R. J., and Bittar, A. (2006). "Sub-wavelength Texturing for Solar Cells using Interferometric Lithography." *Advances in Science and Technology*, 51, 115-120.

Chou, S. Y. (2003). "Nanoimprint Lithography." Alternative Lithography: Unleashing the Potentials of Nanotechnology, C. M. Sotomayor Torres, ed., Kluwer Academic/Plenum Publishers.

Frey, M. D. (2007). "Low kV Scanning Electron Microscopy." Scanning Microscopy for Nanotechnology, W. Zhou and Z. L. Wang, eds., Springer.

Ishii, Y., and Taniguchi, J. (2007). "Fabrication of three-dimensional nanoimprint mold using inorganic resist in low accelerating voltage electron beam lithography." *Microelectronic Engineering*, 84(5-8), 912-915.

ITRS. (2003). "ITRS 2003 Edition." International Technology Roadmap for Semiconductors.

ITRS. (2008). "ITRS 2008 Edition." International Technology Roadmap for Semiconductors.

Joo, J., Chow, B. Y., and Jacobson, J. M. (2006). "Nanoscale Patterning on Insulating Substrates by Critical Energy Electron Beam Lithography." *Nano Lett.*, 6(9), 2021-2025.

Konijn, M., Alkaisi, M. M., and Blaikie, R. J. (2005). "Nanoimprint lithography of sub-100 nm 3D structures." *Microelectronic Engineering*, 78-79, 653-658.

Kumaravelu, G., Alkaisi, M. M., Bittar, A., Macdonald, D., and Zhao, J. (2004). "Damage studies in dry etched textured silicon surfaces." *Current Applied Physics*, 4(2-4), 108-110.

Macintyre, D. S., and Thoms, S. (2005). "A study of resist flow during nanoimprint lithography." *Microelectronic Engineering*, 78-79, 670-675.

Merino, S., Schift, H., Retolaza, A., and Haatainen, T. (2007). "The use of automatic demolding in nanoimprint lithography processes." *Microelectronic Engineering*, 84(5-8), 958-962.

Mohamed, K. (2005). "Resist Deformation in Nanoimprint Lithography (NIL)," Master Degree, University of Canterbury, Christchurch.

Mohamed, K., Alkaisi, M. M., and Blaikie, R. J. (2007). "Fabrication of three dimensional structures for an UV curable nanoimprint lithography mold using variable dose control with critical-energy electron beam exposure." *Journal of Vacuum Science & Technology B: Microelectronics and Nanometer Structures*, 25, 2357-2360.

Mohamed, K., Alkaisi, M. M., and Blaikie, R. J. (2008). "The replication of three dimensional structures using UV curable nanoimprint lithography." *Journal of Vacuum Science & Technology B: Microelectronics and Nanometer Structures*, 26, 2500-2503.

Mohamed, K., Alkaisi, M. M., and Blaikie, R. J. (2009). "Surface charging suppression using PEDOT/PSS in the fabrication of three dimensional structures on a quartz substrate." *Microelectronic Engineering*, 85.

Mohamed, K., Alkaisi, M. M., and Smaill, J. (2006). "Resist deformation at low temperature in nanoimprint lithography." *Current Applied Physics*, 6(3), 486-490.

Romanato, F., Businaro, L., Vaccari, L., Cabrini, S., Candeloro, P., De Vittorio, M., Passaseo, A., Todaro, M. T., Cingolani, R., Cattaruzza, E., Galli, M., Andreani, C., and Di Fabrizio, E. (2003). "Fabrication of 3D metallic photonic crystals by X-ray lithography." *Microelectronic Engineering*, 67-68, 479-486.

Romanato, F., Tormen, M., Businaro, L., Vaccari, L., Stomeo, T., Passaseo, A., and Di Fabrizio, E. (2004). "X-ray lithography for 3D microfluidic applications." *Microelectronic Engineering*, 73-74, 870-875.

Simcic, J., Pelicon, P., Rupnik, Z., Mihelic, M., Razpet, A., Jenko, D., and Macek, M. (2005). "3D micromachining of SU-8 polymer with proton microbeam." *Nuclear Instruments and Methods in Physics Research Section B: Beam Interactions with Materials and Atoms*, 241(1-4), 479-485.

Sun, H., Liu, J., Gu, P., and Chen, D. (2008). "Anti-sticking treatment for a nanoimprint stamp." *Applied Surface Science*, 254(10), 2955-2959.

Taniguchi, J., Koga, K., Kogo, Y., and Miyamoto, I. (2006). "Rapid and three-dimensional nanoimprint template fabrication technology using focused ion beam lithography." *Microelectronic Engineering*, 83(4-9), 940-943.

Thackeray, J. W., Orsula, G. W., Canistro, D., and Berry, A. K. (1989). "Evaluation of Deep UV ANR Photoresist for 248.4 nm Excimer Laser Photolithography." *Journal of Photopolymer Science and Technology*, 2(3), 429-443.

Totsu, K., Fujishiro, K., Tanaka, S., and Esashi, M. (2006). "Fabrication of three-dimensional microstructure using maskless gray-scale lithography." *Sensors and Actuators A: Physical*, 130-131, 387-392.

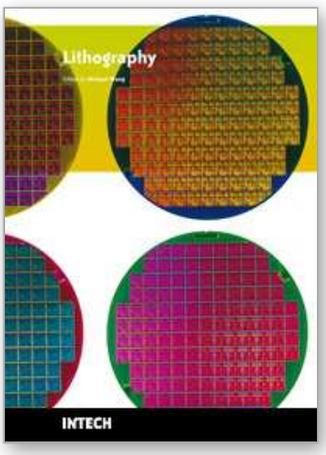

Lithography

Edited by Michael Wang

ISBN 978-953-307-064-3

Hard cover, 656 pages

Publisher InTech

Published online 01, February, 2010

Published in print edition February, 2010

Lithography, the fundamental fabrication process of semiconductor devices, plays a critical role in micro- and nano-fabrications and the revolution in high density integrated circuits. This book is the result of inspirations and contributions from many researchers worldwide. Although the inclusion of the book chapters may not be a complete representation of all lithographic arts, it does represent a good collection of contributions in this field. We hope readers will enjoy reading the book as much as we have enjoyed bringing it together. We would like to thank all contributors and authors of this book.

InTech Europe

University Campus STeP Ri
Slavka Krautzeka 83/A
51000 Rijeka, Croatia
Phone: +385 (51) 770 447
Fax: +385 (51) 686 166
www.intechopen.com

InTech China

Unit 405, Office Block, Hotel Equatorial Shanghai
No.65, Yan An Road (West), Shanghai, 200040, China
中国上海市延安西路65号上海国际贵都大饭店办公楼405单元
Phone: +86-21-62489820
Fax: +86-21-62489821

IntechOpen